2007

Modeling Li/CF_x-SVO Hybrid-Cathode Batteries

Parthasarathy M. Gomadam

Donald R. Merritt

Erik R. Scott

Craig L. Schmidt

Paul M. Skarstad

See next page for additional authors

Publication Info

Journal of the Electrochemical Society, 2007, pages A1058-A1064.

Publisher's link: http://dx.doi.org/10.1149/1.2779963
DOI: 10.1149/1.2779963

Journal of The Electrochemical Society, **154** (11) A1058-A1064 (2007)
0013-4651/2007/154(11)/A1058/7/$20.00 © The Electrochemical Society

Modeling Li/CF_x-SVO Hybrid-Cathode Batteries

Parthasarathy M. Gomadam,[a,*,z] Donald R. Merritt,[a,*] Erik R. Scott,[a,*] Craig L. Schmidt,[a,*] Paul M. Skarstad,[a,*] and John W. Weidner[b,*]

[a]*Medtronic Energy and Component Center, Brooklyn Center, Minnesota 55430, USA*
[b]*Center for Electrochemical Engineering, Department of Chemical Engineering, University of South Carolina, Columbia, South Carolina 29208, USA*

A mathematical model is developed that predicts the voltage-capacity behavior of a primary lithium battery containing a hybrid cathode, which combines the high energy density of carbon monofluoride (CF_x) and the higher power density of silver vanadium oxide (SVO). The model is developed using material balances and kinetic expressions for each material, extracting kinetic and thermodynamic parameters from data collected on CF_x and SVO batteries, and then integrating this information into a hybrid system. The full model is validated by comparing simulations to experimental data on Li/CF_x-SVO hybrid-cathode batteries of various designs and for a range of discharge currents. The model closely agrees with the data up to moderate discharge rates, beyond which the model overpredicts voltage as ignored phenomena (mainly, ohmic resistance) become important.
 [DOI: 10.1149/1.2779963]

Manuscript submitted June 1, 2007; revised manuscript received July 30, 2007. Available electronically September 24, 2007.

Modern implantable medical devices such as pacemakers and neurostimulators offer an ever-increasing array of therapies and features that improve the management of disease states.[1] These features (e.g., increased computational power, sensing and long-distance telemetry) demand the device batteries to be increasingly high-power capable, without compromising on the excellent energy density provided by traditional Li/I_2 batteries. One possible solution, the Li/silver vanadium oxide (SVO) battery, has attractive attributes such as high power density and a stepped voltage-capacity curve with a plateau near the end of discharge. (The latter feature provides an ample and reliable end-of-service warning for device replacement prior to battery depletion.[2-6]) Therefore, the Li/SVO battery is the present state-of-the-art power source for implantable cardioverter defibrillators, which demand peak power loads as high as 10 W from the battery. However, for devices in which such high power is not needed, the Li/SVO battery may be less attractive because its energy density is substantially lower than the Li/I_2 battery. Another possible solution is the Li/CF_x battery, which has comparable energy density to the Li/I_2 battery, although lower power density than the Li/SVO battery. Further, an end-of-service warning is relatively more difficult with the Li/CF_x battery because its voltage-capacity curve remains nearly flat for most of discharge and falls off steeply near the end.

In recent years, Medtronic introduced a battery whose cathode contains a mixture of CF_x and SVO, preserving the best properties of each (namely, high energy and power densities, respectively). This battery, known as the Li/CF_x-SVO hybrid-cathode battery, has comparable energy density to Li/I_2, but with about two orders of magnitude greater power density.[1,7] In addition, the hybrid-cathode battery exhibits the same voltage plateau near the end of discharge as the Li/SVO battery, allowing for a convenient and reliable end-of-service warning. By modulating the mix ratio of CF_x and SVO, one can tune the battery's power-energy characteristic as well as the time interval between end-of-service warning and battery depletion.

To characterize lithium batteries containing hybrid cathodes, a mathematical model was developed that predicts battery performance over a range of design parameters and operating conditions relevant to implantable medical devices. Since these applications typically involve discharges lasting months to years, phenomena having shorter time scales (e.g., capacitance) are ignored in the model, with discharge characteristics being governed by the relative reaction kinetics of the hybrid system. The resulting mathematical model is a set of coupled ordinary differential and algebraic equations that is highly nonlinear, and requires a numerical solution to predict battery performance. To obtain the requisite thermodynamic and kinetic parameters, the model simulations are first fit to discharge data from Li/CF_x and Li/SVO batteries. The model simulations are then compared to discharge curves from Li/CF_x-SVO hybrid-cathode batteries of various mix ratios, electrode thicknesses and geometric areas. Finally, limits on discharge rates and battery design are established, within which the model accurately predicts performance.

* Electrochemical Society Active Member.
z E-mail: partha.m.gomadam@medtronic.com

Experimental

The data used in developing and validating the model were obtained from the batteries listed in Table I. The batteries were all cathode limited but differed in mix ratio, electrode thickness, or geometric area and, therefore, in cathode mass and capacity. The mass and capacity of the active materials are related by Faraday's law, taking into account that CF_x and SVO consume 1 and 6 equivalents of Li, respectively. The maximum capacity is the sum of the individual capacities, and the mix ratio is the ratio of the individual capacities. The cathode is a porous pellet made of CF_x, SVO, and inert materials pressed onto the current collector. The separator is inert porous polyethylene, and the anode is Li metal pressed onto a current collector. The pores of the cathode and separator are flood-filled with electrolyte (1 M $LiBF_4$ in γ-butyrolactone/dimethoxyethane) with excess filling the headspace and other voids in the can.

During operation the batteries were maintained at 37°C and discharged at various currents. For some of the low discharge currents used here, it would have taken years to generate a full voltage-capacity curve. Therefore, to generate these lower-rate discharge curves, sets of batteries were discharged at higher currents to different depths of discharge, after which the current was switched to the given lower value. This resulted in discontinuous discharge curves that were pieced together to form complete discharge curves.

Model Development

Assumptions.— The following assumptions were made in developing the models for Li/CF_x, Li/SVO, and Li/CF_x-SVO hybrid-cathode batteries:

1. The cathode limits battery capacity (i.e., excess Li in anode).
2. The cathode dominates battery resistance (i.e., resistances in the anode and separator are negligible).
3. The cathode is kinetically limited (i.e., ohmic and mass-transfer resistances are negligible) such that the reaction current is uniform throughout the porous electrode.
4. The effects of heat generation, degradation, and parasitic reactions are negligible.
5. The CF_x and SVO particles are spherical and cylindrical, respectively, and of the average sizes given in Tables II and III, respectively.

Table I. Cathode design parameters of the batteries used in this study.

Battery name	Mix-ratio Q_C/Q_{SV}	Thickness L (mm)	Area A (cm^2)	Mass m_C (g)	Mass m_{SV} (g)	Total capacity (Ah)
CF_x	1:0	2.6	5.3	1.908	0.000	1.65
SVO	0:1	2.6	5.3	0.000	5.109	1.38
HB1	7.5:1	2.1	3.1	0.850	0.364	0.83
HB2	7.5:1	2.1	5.0	1.315	0.564	1.29
HB3	2.2:1	2.1	5.0	0.884	1.288	1.11
HB4	7.5:1	2.6	5.3	1.721	0.738	1.69
HB5	7.5:1	8.4	8.3	8.813	3.778	8.64

Equations governing an Li/CF_x battery.— The overall electrochemical reaction occurring at the cathode is[8]

$$CF_x + xLi^+ + xe^- \rightarrow xLiF + C \quad [1]$$

This reaction is irreversible and follows Tafel kinetics as confirmed by our observations of E vs $\ln(I_{app})$ as well as those of Tiedemann[9] and Davis et al.[10] Therefore, the local current density on the surface of a CF_x particle is expressed as

$$i_C = -i_{0C}e^{-\beta_C n_C f(E-U_C)} \quad [2]$$

where U_C is the hypothetical equilibrium potential for CF_x, which is a function of depth of discharge, θ_C. The depth of discharge is related to the reaction current density due to CF_x reduction (i.e., Reaction 1) by Faraday's law as

$$\frac{dm_C}{dt} = \frac{d[m_C^0(1-\theta_C)]}{dt} = \frac{M_C}{n_C F} i_C a_C V \quad [3]$$

where $\theta_C = 0$ at $t = 0$.

As CF_x is consumed via Reaction 1, the surface area available for the electrochemical reaction decreases over the course of discharge. For spherical particles, this area is related to the initial reaction area and the depth of discharge, θ_C, by

$$a_C V = a_C^0 V^0 (1-\theta_C)^{2/3} \quad [4]$$

where the initial reaction area is related to the initial properties of the spherical CF_x particles by

$$a_C^0 V^0 = \frac{3m_C^0}{R_C^0 \rho_C} \quad [5]$$

Combining Eq. 3-5 gives

$$\frac{d\theta_C}{dt} = -\frac{3M_C}{n_C F R_C^0 \rho_C}(1-\theta_C)^{2/3} i_C \quad [6]$$

In general, Eq. 2 and 6 are solved simultaneously to obtain the battery voltage, E, as a function of the depth of discharge, θ_C. For a Li/CF_x battery discharged at constant current, I_{app}, we have

$$I_{app} = i_C a_C V \quad [7]$$

Hence, combining Eq. 3 and 7 and integrating gives a linear relationship between θ_C and time. Also, substituting Eq. 2 and 4 into Eq. 7 and rearranging gives the battery voltage as

$$E = \left[U_C + \frac{1}{\beta_C n_C f} \ln(a_C^0 V^0 i_{0C}) \right] - \frac{1}{\beta_C n_C f} \ln\left(\frac{-I_{app}}{(1-\theta_C)^{2/3}} \right) \quad [8]$$

The bracketed term in Eq. 8 is an unknown function of θ_C, and β_C is an unknown constant. Equation 8 can be fit to discharge data from a Li/CF_x battery to obtain these quantities.

Equations governing an Li/SVO battery.— According to Crespi et al.,[6] the overall reaction occurring at the SVO electrode is

$$Ag_2^+V_4^{5+}O_{11} + (x+y)Li^+ + (x+y)e^- \rightarrow Li_{x+y}^+ Ag_{2-x}^+ V_y^{4+} V_{4-y}^{5+} O_{11} + xAg^0 \quad [9]$$

in which Li insertion is accompanied by silver and vanadium reductions. The open-circuit potential vs depth-of-discharge curve measured for the Li/SVO battery has two plateaus: one at 3.2 V, corresponding to the phase-change reduction of Ag^+ to Ag and the other

Table II. Parameters in Li/CF_x battery model.

Parameter	Value	Remarks
ρ_C	2.75 g/cm^3	Measured
M_C	31.0 g/mol	For $x \approx 1$
n_C	1	Stoichiometry
R_C^0	10 μm	Measured
β_C	0.57	Estimated from data

Table III. Parameters in Li/SVO battery model.

Parameter	Value	Remarks
β_S	0.5	Assumed
β_V	0.5	Assumed
ρ_{SV}	4.789 g/cm^3	Measured
M_{SV}	595.5 g/mol	
n_S	2	Stoichiometry
n_V	4	Stoichiometry
R_{SV}^0	1 μm	Measured
k_S	10^{-10} A/cm^2	Estimated
i_{0V}	10^{-8} A/cm^2	Estimated
U_S	$0.156\exp(-20.0\theta_S) + \frac{(3.84 + 1050\theta_S - 288\theta_S^2 - 418\theta_S^3 + 116\theta_S^4 + 17.1\theta_S^5)}{(1 + 325\theta_S - 91.7\theta_S^2 - 126\theta_S^3 + 34.4\theta_S^4 + 5.49\theta_S^5)}$	Fit of higher-voltage plateau of Fig. 2
U_V	$0.823\exp(-20.0\theta_V) + \frac{(3.18 + 5.80\theta_V^2 + 0.192\theta_V^4 - 0.161\theta_V^6 + 0.00900\theta_V^8)}{(1 + 2.46\theta_V^2 - 0.0246\theta_V^4 - 0.0419\theta_V^6 + 0.00162\theta_V^8 + 0.0000628\theta_V^{10})}$	Fit of lower-voltage plateau of Fig. 2

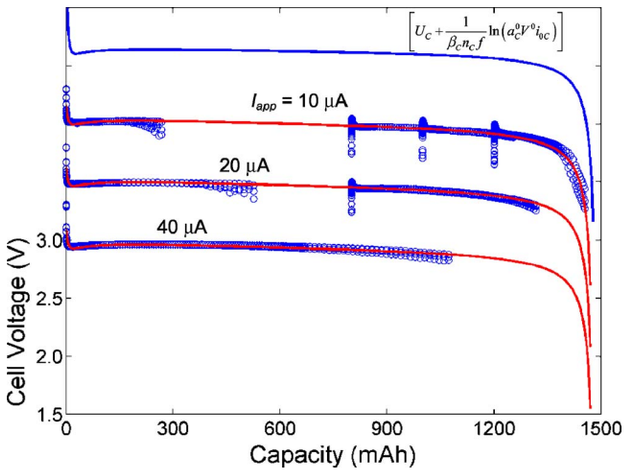

Figure 1. (Color online) Model simulations fit to discharge data obtained from Li/CF_x batteries. The parameters resulting from the fit are the bracketed term in Eq. 8 and $\beta_C = 0.57$. The functional form of the bracketed term is given in Eq. 19 and plotted above. For clarity, the curves for 20 μA, 10 μA and the bracketed term are shifted up from the 40 μA curve by 0.5, 1.0 and 1.5 V, respectively.

at 2.6 V, corresponding to the reduction of V^{5+} to V^{4+}. Further, discharge data from Li/SVO batteries show very different resistances associated with these two regions of the voltage curve. To incorporate these effects in the model, the SVO reduction reaction is treated mathematically as if it is a parallel combination of the reduction reaction of silver as given by

$$Ag_2^+V_4^{5+}O_{11} + xLi^+ + xe^- \rightarrow Li_x^+Ag_{2-x}^+V_4^{5+}O_{11} + xAg^0 \quad [10]$$

and the reduction of vanadium as given by

$$Ag_2^+V_4^{5+}O_{11} + yLi^+ + ye^- \rightarrow Li_y^+Ag_2^+V_y^{4+}V_{4-y}^{5+}O_{11} \quad [11]$$

It is important to note that these reactions may take place simultaneously. Although a simplification, this approach allows for accurate computation of the kinetic resistance associated with SVO reduction.

The overall depth of discharge of the SVO electrode is defined as the sum of the depths of discharge, θ_S and θ_V, of silver reduction (Eq. 10) and vanadium reduction (Eq. 11), respectively. These individual depths of discharge are defined as the values that x and y can take in Reactions 10 and 11, respectively, at any time during discharge. In a fully charged SVO electrode, these values are zero, and in a fully discharged electrode θ_S reaches 2 and θ_V reaches 4. Assuming Butler-Volmer kinetics holds for both silver and vanadium reductions, we get

$$i_S = i_{0S}\left[e^{\beta_S n_S f(E-U_S)} - e^{-(1-\beta_S)n_S f(E-U_S)}\right] \quad [12]$$

$$i_V = i_{0V}\left[e^{\beta_V n_V f(E-U_V)} - e^{-(1-\beta_V)n_V f(E-U_V)}\right] \quad [13]$$

where U_S and U_V are the depth-of-discharge-dependent equilibrium potentials for silver and vanadium reductions, respectively.

Unlike CF_x, the reaction surface area for the cylindrical SVO is constant throughout the discharge and is given by

$$a_{SV}V = a_{SV}^0V^0 = \frac{2m_{SV}^0}{R_{SV}^0\rho_{SV}} \quad [14]$$

Writing analogous material balances for silver oxide and vanadium oxide as was done for CF_x (Eq. 3), and combining with Eq. 14 gives

$$\frac{d\theta_S}{dt} = -\frac{2M_{SV}}{n_S F R_{SV}^0 \rho_{SV}} i_S \quad [15]$$

$$\frac{d\theta_V}{dt} = -\frac{2M_{SV}}{n_V F R_{SV}^0 \rho_{SV}} i_V \quad [16]$$

where $\theta_S = \theta_V = 0$ at $t = 0$.

For an Li/SVO battery discharged at a constant current, I_{app}, we have

$$I_{app} = (i_S + i_V)a_{SV}V \quad [17]$$

Equations governing an Li/CF_x-SVO hybrid-cathode battery.— Since the reduction currents of the component materials are additive, the three material balances (Eq. 6, 15, and 16) and the three kinetic expressions (Eq. 2, 12, and 13) are solved simultaneously to give the battery voltage as a function of the overall depth of discharge or capacity of the battery. For constant current discharge, the applied current is related to the reaction currents by

$$I_{app} = i_C a_C V + (i_S + i_V)a_{SV}V \quad [18]$$

The differential-algebraic equations of the models presented above are solved using Comsol, a commercial numerical software package. For each battery shown in Table I, the equations are solved to calculate the battery voltage, E, as a function of time (i.e., depth of discharge or capacity) for a given discharge current, I_{app}.

Results and Discussion

The Li/CF_x Battery.— Equation 8, in conjunction with Eq. 3 and 7, is fit to the discharge data for Li/CF_x batteries (see design parameters in Table I and physical parameters in Table II) at 10, 20, and 40 μA. The statistical fit, using the commercial software TableCurve 2D, gives the bracketed term in Eq. 8 as an empirical function of θ_C as

$$\left[U_C + \frac{1}{\beta_C n_C f}\ln(a_C^0 V^0 i_{0C})\right] = -0.551 + \frac{(5.57 - 1.48\times10^3\theta_C + 2.40\times10^5\theta_C^2 - 1.10\times10^5\theta_C^3 - 1.69\times10^5\theta_C^4)}{(1 - 4.04\times10^2\theta_C + 7.57\times10^5\theta_C^2 - 3.21\times10^4\theta_C^3 - 5.55\times10^4\theta_C^4)} \quad [19]$$

along with $\beta_C = 0.57$. Figure 1 shows the comparison between the model simulations (lines) and experimental data (circles). Equation 19 is also plotted in Fig. 1. Note that the curves are offset from each other by 0.50 V for better clarity in comparing the data and simulations, with the 40 μA discharge having no offset. The discontinuity in some of the discharge data results from sets of batteries discharged at higher currents to different depths of discharge, after which the current was switched to the given lower value. The full discharge curve was then pieced together to form the discharge curves shown in Fig. 1. For the statistical fit described above, the data collected during the transition from high rate to low rate discharge were not used.

The Li/SVO battery.— Figure 2 shows the open-circuit potential curve measured by Crespi et al.[6] as a function of the quantity $(x + y)$ in Reaction 9, which is equivalent to the sum of the depths of discharge of the silver and silver reduction reactions, $(\theta_S + \theta_V)$.

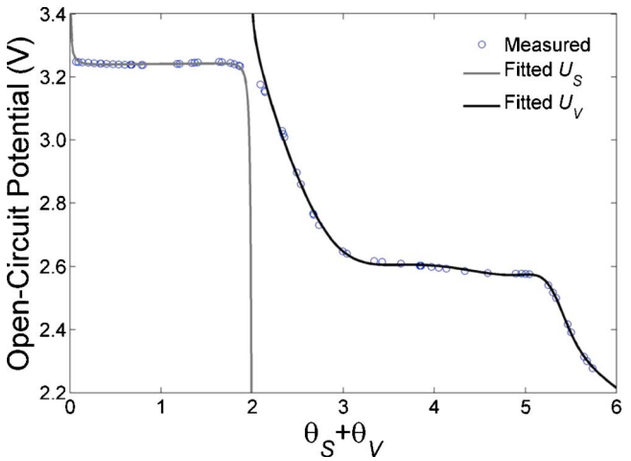

Figure 2. (Color online) Measured open-circuit potential of SVO reported by Crespi et al. (Ref. 4) (circles). The data are split into the open-circuit potentials for silver and vanadium reductions, U_S and U_V, and fitted as functions of depths of discharge, θ_S and θ_V, respectively.

This curve is split into two curves: one spanning the region 0–2 on the x axis and the other spanning 2–6. The first part is treated as the open-circuit potential for the hypothesized silver reduction (i.e., Reaction 10) and fit as a function of its depth of discharge, θ_S, ranging from 0 to 2. The second part is treated as the open-circuit potential for the hypothesized vanadium reduction (i.e., Reaction 11) and fit as a function of its depth of discharge, θ_V, ranging from 0 to 4. The statistical fits, using the commercial software TableCurve 2D, are given in Table III.

Using the expressions for U_S and U_V from Table III, the material balances (Eq. 15 and 16), the kinetic expressions (Eq. 12 and 13), are solved along with Eq. 14 and 17 and fit to the discharge data for Li/SVO batteries (see design parameters in Table I and physical parameters in Table III at 5 through 1000 μA). The unknown parameters involved are the transfer coefficients (β_S and β_V) and the exchange-current densities (i_{0S} and i_{0V}). The values of the transfer coefficients do not affect the voltage-capacity curves significantly and, therefore, they are set to 0.5. The measured voltage at the lower plateau shows little change with current, which means that the kinetics of vanadium reduction is fast. This gives a lower limit of 10^{-8} A/cm^2 for i_{0V}. The upper plateau, however, varies strongly with current, which was fit to

$$i_{0S} = k_S(2 - \theta_S)^2 \qquad [20]$$

to obtain $k_S = 10^{-10}$ A/cm^2. Figure 3 shows the comparison between the model simulations (lines) and the experimental data (symbols). Again, the discontinuity in some of the discharge data results from piecing together sets of discharge curves. For the statistical fit described above, the data collected during the transition from high rate to low rate discharge were not used.

The Li/CF$_x$-SVO hybrid-cathode battery.— The material balances (Eq. 3, 15, and 16), the kinetic parameters (Eq. 2, 12, and 13) and Eq. 5, 14, and 18 are solved simultaneously to generate discharge curves at various currents for the five hybrid-cathode batteries shown in Table I. The parameters estimated above with Li/CF$_x$ and Li/SVO batteries are used to simulate the discharge curves with no additional parameters fit to the data. The comparisons between model simulations (lines) and experimental data (symbols) for the five hybrid-cathode batteries are shown in Fig. 4-7. Excellent agreement is observed for hybrid-cathode batteries HB1 through HB4 at all currents shown (Fig. 4-6).

For the largest battery (HB5), good agreement is observed below 800 μA, but deviations in both voltage and capacity are observed at higher currents (Fig. 7). At higher current densities, voltage drop in the low-conducting electrolyte phase of the porous cathode becomes significant, resulting in nonuniform reaction current distributions. This invalidates the assumption of uniform reaction current distribution and purely kinetic limitations (i.e., assumption 3).

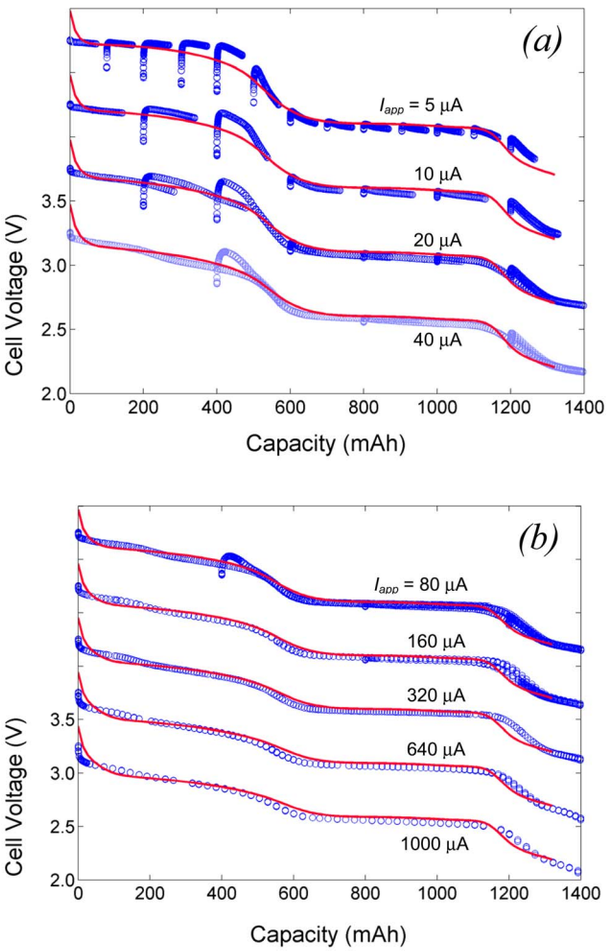

Figure 3. (Color online) Model simulations fit to discharge data obtained from Li/SVO batteries for (a) 5–40 μA and (b) 80–1000 μA. The parameters resulting from the fit are listed in Table III. In part (a), the curves for 20, 10 and 5 μA are shifted up from the 40 μA curve by 0.5, 1.0 and 1.5 V, respectively. In part (b), the curves for 640, 320, 160 and 80 μA are shifted up from the 1000 μA curve by 0.5, 1.0, 1.5 and 2.0 V, respectively.

The design and operating region for which assumption 3 is valid can be determined by applying porous electrode theory.[11] Since the porous cathode is largely CF$_x$, which obeys Tafel kinetics, the uniformity of reaction is governed by the ratio of the effective ohmic resistance of the cathode to the applied current density. This quantity is captured by the parameter $\delta \equiv f\beta_C I_{app} L(1/\kappa + 1/\sigma)/A$, which reduces to $\delta = f\beta_C I_{app} L/A\kappa$, as the ionic conductivity is much lower than the electronic conductivity. The lower the value of δ, the lower the ohmic limitation and the more uniform the reaction distribution. Since the model presented here assumes uniform reaction distribution and purely kinetic limitation, its validity decreases with increasing value of δ. Based on the comparisons presented here, we see that the model predictions match experimental data when $\delta < 10$ ($\kappa = 10^{-4}$ S/cm). Deviations in the model are observed for the HB5 batteries discharging at 400 μA or higher, when $\delta > 10$ (Fig. 7).

Note that the model requires only the masses of CF$_x$ and SVO active materials, which are provided in Table I for all cases considered. The compositions and properties of binder and conductivity

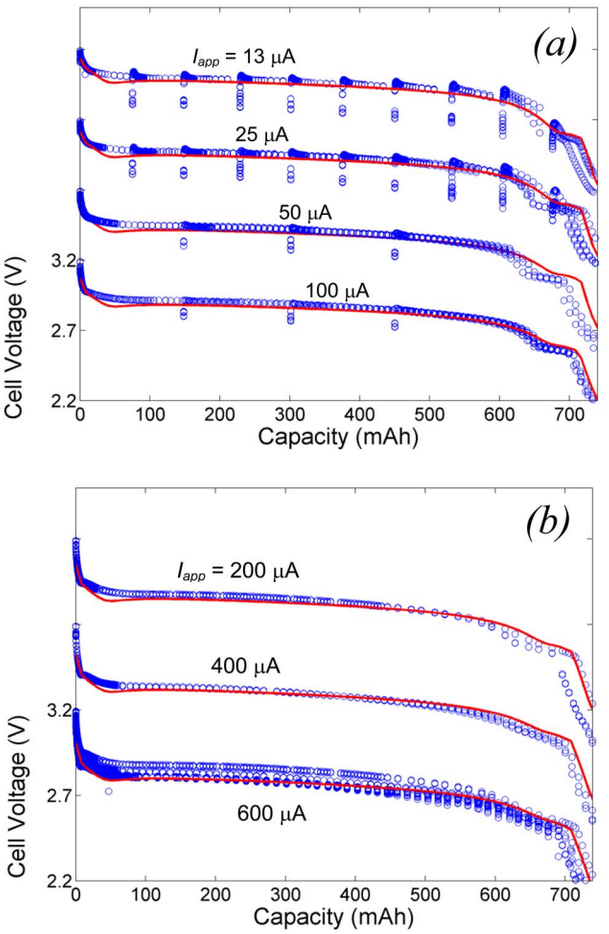

Figure 4. (Color online) Comparison between model predictions and discharge data obtained from the HB1 batteries for: (a) 13–100 μA and (b) 200–600 μA. In part (a), the curves for 50, 25 and 13 μA are shifted up from the 100 μA curve by 0.5, 1.0 and 1.5 V, respectively. In part (b), the curves for 400 and 200 μA are shifted up from the 600 μA curve by 0.5 and 1.0 V, respectively.

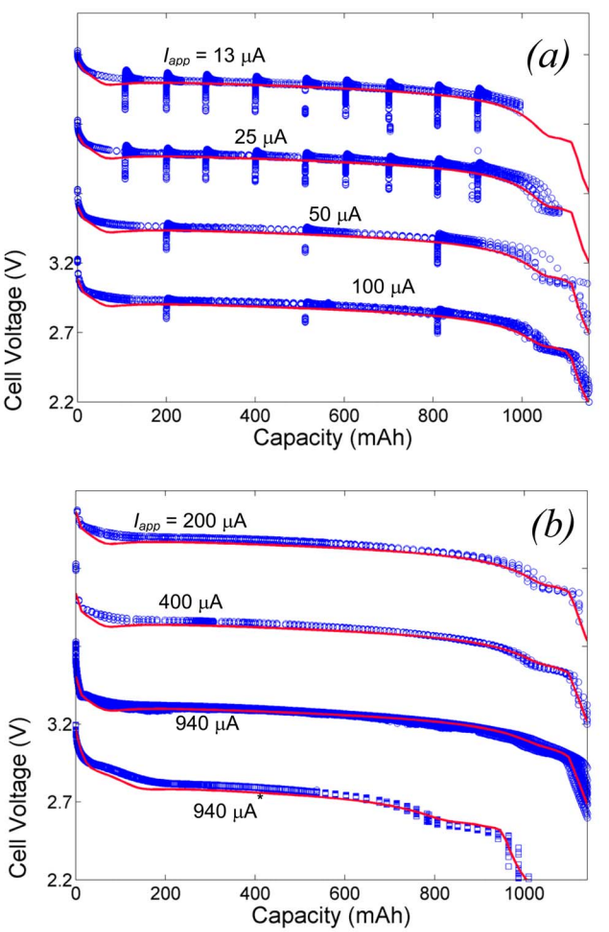

Figure 5. (Color online) Comparison between model predictions and discharge data obtained from the HB2 batteries for (a) 13–100 μA and (b) 200–940 μA; and HB3 batteries for: (b) 940 μA*. In part (a), the curves for 50, 25 and 13 μA are shifted up from the 100 μA curve by 0.5, 1.0 and 1.5 V, respectively. In part (b), the curves for 940, 400 and 200 μA are shifted up from the 940 μA* curve by 0.5, 1.0 and 1.5 V, respectively.

aid do not matter as long as the effective electronic conductivity of the cathode is sufficiently large so that δ is less than 10.

Effect of current on component depths of discharge (θ_C, θ_S, θ_V).— The model is used to study the effect of current on the time-variation of the depths of discharge of the components of the hybrid cathode. Two cases are considered, namely, a low-current case when the battery operates closer to equilibrium, and a high-current case, when the battery operates farther from equilibrium. The predicted component depths of discharge of silver reduction (θ_S), CF_x reduction (θ_C), and vanadium reduction (θ_V) are shown in Fig. 8a. The predicted battery voltages for the two currents are shown in Fig. 8b. The abscissa in the figure is the depth of discharge of the battery, defined as $-I_{app}t/(Q_C + Q_{SV})$. The simulations are for the case of the HB2 battery discharging at 1 and 1000 μA. However, for given initial specific surface areas of CF_x and SVO (a_C and a_{SV}) the curves in Fig. 8 are governed only by two parameters: $-I_{app}/(Q_C + Q_{SV})$ and the mix ratio, m ($\equiv Q_C/Q_{SV}$). The order of the reactions and the shape of the voltage curve are determined by the relative polarizations experienced by the individual components, which in turn depend on the individual equilibrium potentials and reaction kinetics.

For the low-current case, silver and vanadium reductions occur for about the first 10% of discharge until silver reduction reaches near completion (i.e., $\theta_S \rightarrow 2$). This brings the battery voltage down to values where CF_x reduction begins and its depth of discharge (θ_C) starts to increase. Over the next 70% of discharge, θ_C increases while θ_S and θ_V remain nearly constant. At about 80% battery depth of discharge, θ_C reaches a value of about 0.9 bringing the battery voltage down to values where vanadium reduction begins to occur. Beyond this point, θ_S and θ_C remain nearly constant while θ_V increases, supplying the next 10% of discharge capacity. When battery depth of discharge reaches a value of about 0.9, vanadium reduction reaches near completion (i.e., $\theta_V \rightarrow 4$) bringing the battery voltage down to the cutoff value of 2.2 V. Note that CF_x alone provides about 70% of the discharge capacity as the hybrid cathode considered here is predominantly CF_x (HB2 battery, mix ratio = 7.5:1).

The same order of reactions is maintained for the high-current discharge except that vanadium reduction supplies a greater fraction of the battery capacity initially. During the first 10% of discharge, θ_V reaches a higher value in the high-current case, a result of vanadium reduction being significantly faster than silver and CF_x reductions. For the same reason, the difference in the battery voltages for the high and low currents is large except in the last 10% of discharge, where nearly all the capacity is supplied by vanadium reduc-

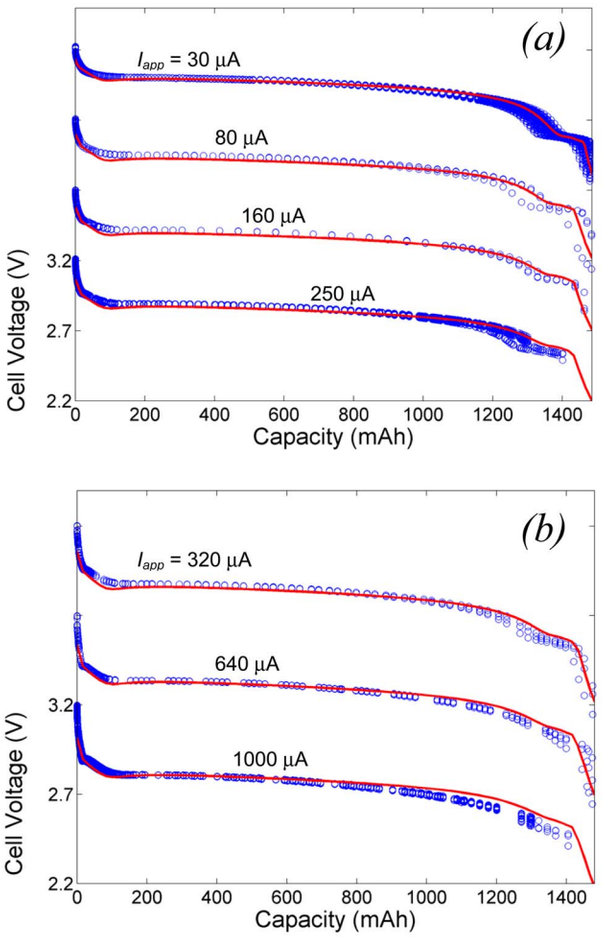

Figure 6. (Color online) Comparison between model predictions and discharge data obtained from the HB4 batteries for (a) 30–250 μA and (b) 320–1000 μA. In part (a), the curves for 160, 80 and 30 μA are shifted up from the 250 μA curve by 0.5, 1.0 and 1.5 V, respectively. In part (b), the curves for 640 and 320 μA are shifted up from the 1000 μA curve by 0.5 and 1.0 V, respectively.

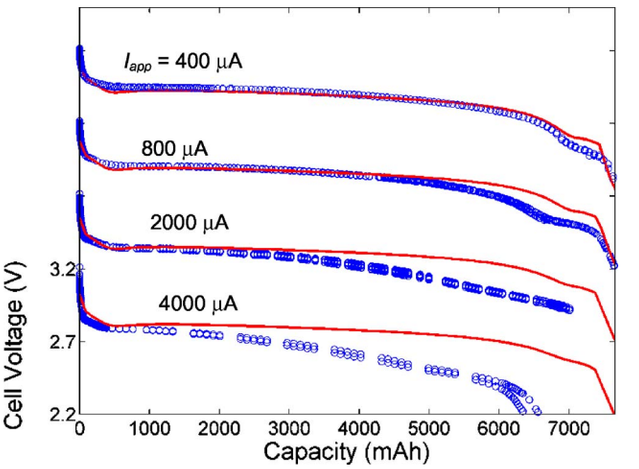

Figure 7. (Color online) Comparison between model predictions and discharge data obtained from the HB5 batteries for 400–4000 μA. The curves for 2000, 800 and 400 μA are shifted up from the 4000 μA curve by 0.5, 1.0 and 1.5 V, respectively.

tion. The greater polarization in the high-current case causes the battery to reach cutoff voltage before vanadium reduction is complete (i.e., before θ_V reaches 4).

Conclusion

A mathematical model is developed that predicts the voltage-capacity behavior of a primary lithium battery containing a hybrid cathode. The model is developed using the material balances and kinetic expressions for CF_x and SVO, extracting kinetic and thermodynamic parameters from data collected on Li/CF_x and Li/SVO batteries, and then integrating this information into a hybrid system. The full model is validated by comparing simulations to experimental data on hybrid-cathode batteries of various designs and for a range of discharge currents. The ratio of cathode ionic resistance to the applied current density, δ, is identified as the parameter governing the validity range of the model. For battery designs and operating currents such that $\delta < 10$, close agreement is observed between experimental data and model simulations. In the case of thick electrodes operating at high currents (i.e., when $\delta > 10$), ohmic resistance is important, the reaction in the porous electrode is nonuniform, and the model overpredicts battery voltage and delivered capacity. Including ohmic resistance in the model makes it somewhat more mathematically intensive, and will be the subject of future work by our group.

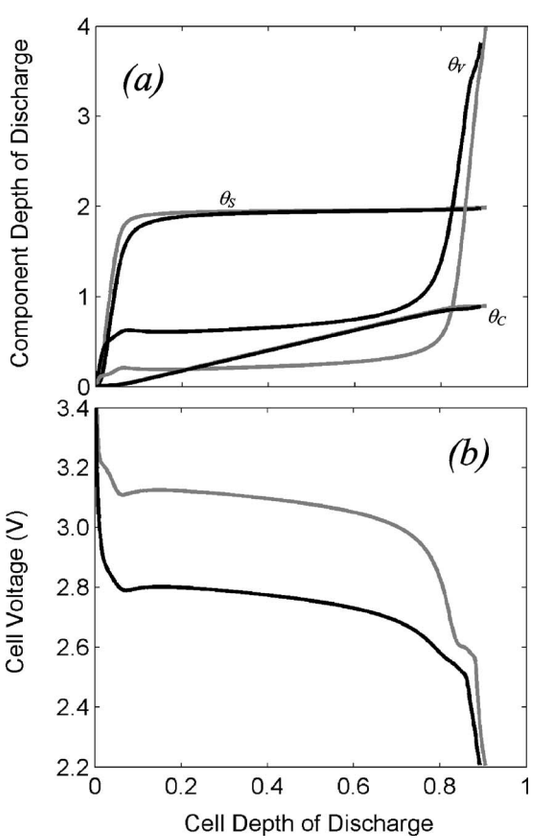

Figure 8. Predicted effect of discharge current on (a) depths of discharge of the components of the hybrid cathode and (b) battery voltage. The gray lines are for 1 μA and the black lines are for 1000 μA discharge of the HB2 battery. The abscissa is the depth of discharge of the battery, defined as $-I_{app}t/(Q_C + Q_{SV})$.

Medtronic Incorporated assisted in meeting the publication costs of this article.

List of Symbols

a	specific surface area of electrode, cm^2/cm^3
A	geometric area of electrode, cm^2
E	battery voltage, V
f	constant, 37.44 V^{-1}
F	constant, 96487 C/mol
i	current density, A/cm^2
i_0	exchange-current density, A/cm^2
I_{app}	current, A
k	rate constant, A/cm^2
L	cathode thickness, cm
m	mass, g
M	molecular weight, g/mol
n	number of electrons transferred per mole
Q	total theoretical capacity, C
R	particle radius, cm
t	time, s
U	open-circuit voltage, V
V	cathode volume, cm^3

Greek

β	transfer coefficient
δ	parameter governing reaction current distribution, defined as $f\beta_C I_{app} L/A\kappa$
θ	depth of discharge
ρ	macroscopic density, g/cm^3
σ	effective electronic conductivity of the cathode, S/cm
κ	effective ionic conductivity of the cathode, S/cm

Subscripts

C	carbon monofluoride (CF_x)
S	silver
SV	silver vanadium oxide (SVO)
V	vanadium

Superscripts

0	initial
max	maximum

References

1. K. Chen, D. R. Merritt, W. G. Howard, C. L. Schmidt, and P. M. Skarstad, *J. Power Sources*, **162**, 837 (2006).
2. E. R. Scott, C. L. Schmidt, and P. M. Skarstad, *Encyclopedia of Biomaterials and Biomedical Engineering*, p. 816, Dekker, New York (1987).
3. E. S. Takeuchi and W. C. Thiebolt, *J. Electrochem. Soc.*, **135**, 2691 (1988).
4. A. M. Crespi, P. M. Skarstad, and H. W. Zandbergen, *J. Power Sources*, **54**, 68 (1995).
5. K. West and A. M. Crespi, *J. Power Sources*, **54**, 334 (1995).
6. A. Crespi, C. Schmidt, J. Norton, K. Chen, and P. Skarstad, *J. Electrochem. Soc.*, **148**, A30 (2001).
7. D. J. Weiss, J. W. Cretzmeyer, A. M. Crespi, W. G. Howard, and P. M. Skarstad, U.S. Pat. 5,180,642 (1993).
8. T. Nakajima and N. Watanabe, *Graphite Fluorides and Carbon-Fluorine Compounds*, CRC, Boca Raton, FL (1991).
9. W. Tiedemann, *J. Electrochem. Soc.*, **121**, 1308 (1974).
10. S. Davis, E. S. Takeuchi, W. Tiedemann, and J. Newman, *J. Electrochem. Soc.*, **154**, A477 (2007).
11. J. S. Newman and K. E. Thomas-Alyea, *Electrochemical Systems*, 3rd ed., Wiley, New York (2004).